Dunakavics

Dunakavics

Tartalom

ANDRÁS NAGY *–ATTILA SZABÓ **–DÁNIEL KÓTI ***–GÁBOR LADÁNYI ****

Apparatus for measuring magnetic properties of thin amorphous ribbons

Abstract: It is very important to accurately measure magnetic properties of ferrous materials in the development of improved electric motors and generators. The pure magnetic properties of new generation amorphous materials show better performance, however forming or cutting the base material decreases these excellent properties because of the mechanical and/or thermal stress caused by the cutting technology. To allow development of the adequate cutting technology for amorphous materials, the effect of cutting on the magnetic properties need to be determined. This can be done by developing a specialized instrument that is capable to accurately measure magnetic properties of small sized amorphous ribbons. This paper introduces the main challenges in the development. Generation of strong magnetic field for the excitation of the specimen is required while small B field is measured in the same place and in the same time, which makes the system quite sensitive to design, building accuracy and calibration.

Keywords: B-H curve measurement, instrumentation, amorphous material.

* *Dunaújvárosi Egyetem, Műszaki Intézet*
E-mail: nagy.andras@uniduna.hu

** *Dunaújvárosi Egyetem, Műszaki Intézet*
E-mail: szaboattila@uniduna.hu

*** *Dunaújvárosi Egyetem, Műszaki Intézet*
E-mail: koti.daniel@uniduna.hu

**** *Dunaújvárosi Egyetem, Műszaki Intézet*
E-mail: ladanyi@uniduna.hu

Absztrakt: A következõ generációs elektromotorok és generátorok fejlesztése során nagy hangsúlyt kell fektetni a mágneses tulajdonságok pontos meghatározására. Az újfajta amorf szerkezeti anyagok mágneses tulajdonságai túlszárnyalják a hagyományosan alkalmazott szerkezeti anyagokét, habár a megmunkálás során ezek a kiváló mágneses tulajdonságok romlanak a megmunkálás mechanikai vagy hõtani terhelései miatt. A megfelelõ megmunkálási (kivágási) technológiák fejlesztésének elõsegítése végett szükség van arra, hogy a megmunkálás az anyag mágneses tulajdonságaira gyakorolt hatását mérés segítségével, nagy pontossággal meg lehessen határozni. Erre a célra egyedi mérõrendszer fejlesztése szükséges, amely ki térfogatú anyagminták mágneses tulajdonságainak nagy pontosságú meghatározására képes. Ez a

[1] Men, H., et.al. (2009): *Fe-Rich Soft Magnetic FeSiBPCu Hetero-Amorphous Alloys with High Saturation Magnetization, Materials Transactions.* Vol. 50, No. 6. Pp. 1330–1333.

cikk egy ilyen berendezés fejlesztésének kihívásait gyûjti össze, illetve bemutatja a tervezés és építés lépéseit. Részleteket szolgáltat továbbá néhány méretezési kihívás megoldásáról és a Dunaújvárosi Egyetemen folyó fejlesztés aktuális állapotáról.

Kulcsszavak: B-H görbe mérés, műszer, amorf anyag.

Introduction

In the recent paper, some of the key challenges in the development of magnetic property measurements of materials are described. The research is driven by the global intention to increase the efficiency of electric motors. This is part of the recent developments of electric vehicles, and aims to make electric vehicles more efficient and environment friendly. Improving vehicle efficiency causes significant reduction of global energy consumption, since the amount of energy consumed by transportation is around one third of the global consumption.

To further improve the efficiency of electric motors, new materials need to be introduced in the production that have better magnetic properties. One group of materials that is expected to contribute in this improvement is the soft magnetic amorphous materials. FeSiB amorphous alloys are widely spread thanks to its low cost and very high saturation magnetization. The Fe-based amorphous and hetero-amorphous alloys shows low intrinsic magnetocrystalline anisotropy and therefore are regarded as substitutes for the silicon steel in the future applications. [1]

Amorphous materials come in the form of thin foil. The thickness is usually 20–40μm, and the foil can be as wide as 100 mm. The excellent magnetic properties of these materials, however, is degraded by mechanical or thermal stress of cutting. To produce the suitable shape that is used in manufacturing the electric motor, cutting of the base material is essential.

This work is part of the overall research that aims to find the balance between the mechanical and magnetic properties of amorphous materials in terms of cutting technology. To enable the accurate measurements required for this research program, a specialized, task-oriented measurement system is developed. This paper describes the challenges arise when such system is designed.

The measurement system consists of a solenoid, coil driving and data acquisition electronics, PC control software and magnetic field sensors (magnetometer).

The magnetometer used is a fluxgate magnetometer that is capable to measure two magnitude weaker magnetic fields than the earth magnetic field, hence makes accurate measurement of small specimen possible. The solenoid is used to generate the excitation (H-field) for the specimen investigated. The main challenge is to accurately set the strength of this magnetic field, since it has direct effect on the results.

Theory of operation

Magnetic field − magnetic properties

The essential practical characteristic of any ferromagnetic material is the irreversible nonlinear response of magnetization M to an imposed magnetic field H. This response is epitomized by the hysteresis loop, as shown in *Figure 1*. [2]

Fig. 1. Typical hysteresis loop of a ferromagnet [2]
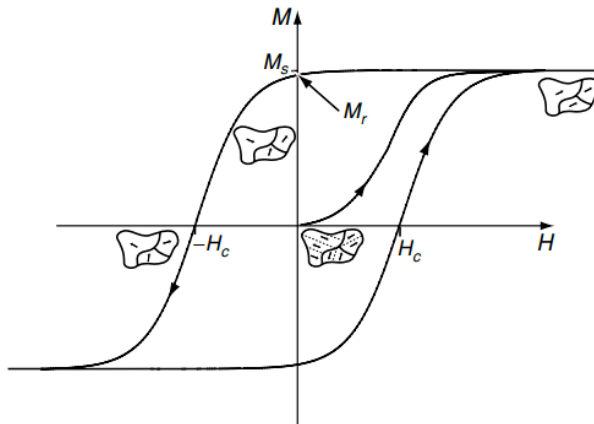
There are two basic types of magnetometers: vector and scalar magnetometers. The former measures the vector components of the magnetic field, while the latter measures the magnitude only.

[2] Coey, J. M. D. (2010): Magnetism and Magnetic Materials, *Cambridge University Press*.

[3] Edelstein, A. (2014): Advances in magnetometry. J. Phys.: *Condens. Matter.* 19 (16). Pp. 28.

[4] Buschow, K. H. J.–De Boer, F. R. (2004): Physics of Magnetism and Magnetic Materials. *Kluwer Academic Publishers.*

The main types are [3]:
1. Scalar magnetometers:
   – Proton precession magnetometer
   – Overhauser effect magnetometer
   – Caesium vapour magnetometer
   – Potassium vapour magnetometer
2. Vector magnetometers:
   – Rotating coil magnetometer
   – Hall effect magnetometer
   – Magnetoresistive devices
   – Fluxgate magnetometer
   – SQUID magnetometer
   – Spin-exchange relaxation-free (SERF) atomic magnetometers

For the application described in this paper, vector magnetometer is required, because they offer an additional way to eliminate any external magnetic field comes from the environment.

Fig. 2. Comparison of magnetometers [4]
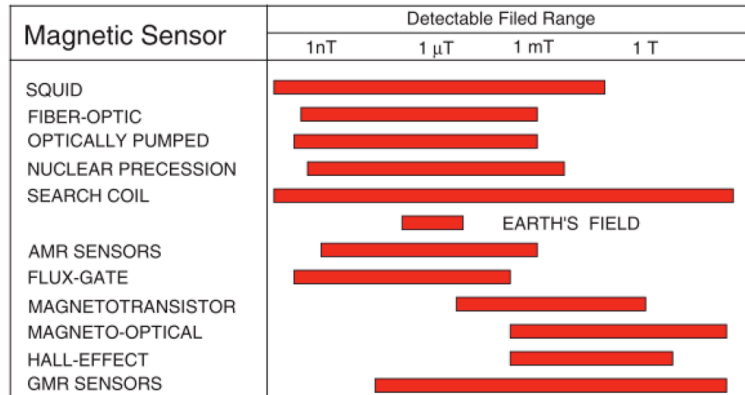
Figure 2 shows a comparison of common magnetometers in terms of detectable field strength. It is expected, that the amorphous specimen, with its

size and material property, will generate B-field in the order of 0.1µT. Therefore adequate magnetic sensor technology needs to be applied to make the measurement accurate. The suitable magnetometers are the squid, the fluxgate and the SERF. All of them offer better than 50 nT accuracy and less than 30pT/√Hz noise, however the fluxgate sensor has significantly lower price than the others. Based on these aspects, we chose the fluxgate magnetometer to detect the B-field of the specimen in the instrument.

The operation of the fluxgate magnetometer is based on the fluxgate effect. Classical fluxgate sensors consist of two identical ferromagnetic cores that are driven into deep saturation. The two parallel bars of a ferromagnetic material (establishes the axis direction) are placed together as close as possible. Each bar is wound with a primary coil, but the direction in which the coil is wrapped around the bars is reversed, see *Figure 3* for explanation. [5]

Fig. 3. Arrangement of classical fluxgate sensor and its waveforms [5]

[5] In, V.–Longhini, P.–Palacios, A. (2009): *Applications of Nonlinear Dynamics, Model and Design of Complex Systems*. Springer.
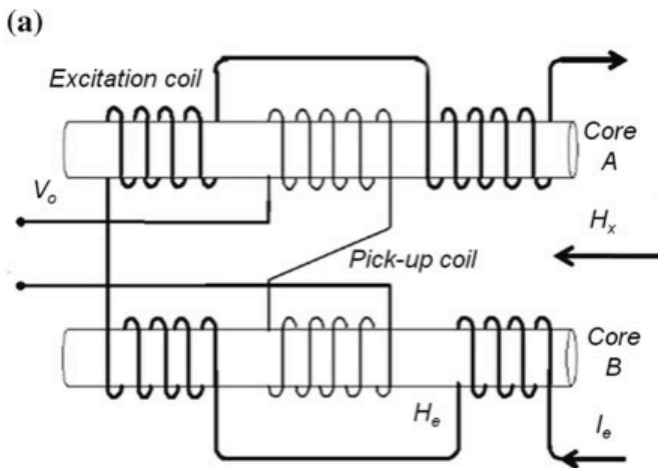
[6] Matsuoka, et.al. (2013): *Development of fluxgate magnetometers and applications to the space science missions, An Introduction to Space Instrumentation.* Oyama, K.–Cheng. C, Z. (Eds.) Pp. 217–225. Terrapub.

[7] Takahashi, T. (2013): *Magnetic Field Measurement (MFM) and Sun Aspect Sensor (SAS), An Introduction to Space Instrumentation.* Oyama, K.–Cheng. C, Z. (Eds.) Pp. 165–179. Terrapub.
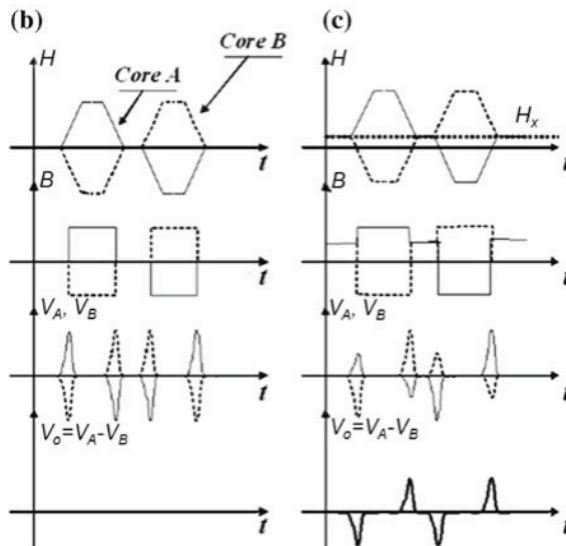
Fluxgate magnetometers are used widely in space probe applications and earth magnetic surveys, for which there are several examples in the literature. [6, 7]

Measurement technique

The magnetic properties that need to be measured by the system, originated from the BH curve, therefore the main objective is to accurately determine the BH curve of the specimen. For that purpose, the H field is generated and the B filed is measured with high accuracy. The H field is generated with solenoid, so that the specimen in the axis of the coil is excited by homogenous magnetic filed. In this arrangement, the B field sensor is positioned half way close to the solenoid, which makes it possible to measure the tiny B field in the presence of strong H field. In Figure 4 this arrangement can be seen.

Fig. 4: Arrangement of the solenoid, specimen and the magnetometer
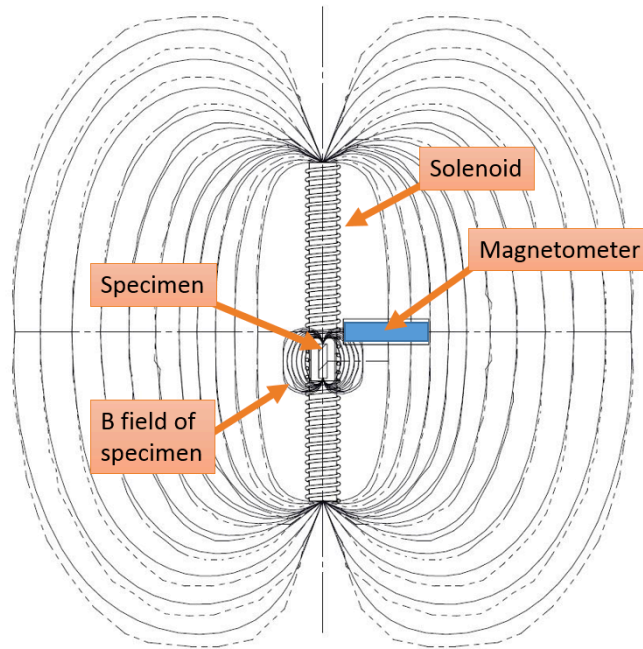
The figure also shows, that the B field of the specimen, generated by the excitation H field, is measured in the middle of the solenoid where the H field is the weakest.

Instrument development

SPECIFICATIONS

In order to adequately develop the instrument for the specific application described in the introduction, the main parameters need to be carefully specified. As shown in Chapter 2.3, the main components of the instrument are the excitation solenoid, the magnetometers, the control and acquisition electronics and the PC software.

The biggest components in terms of size is the solenoid, which generates the H-field for the measurement of B-H curve. Its geometry needs to satisfy several requirements determined by the size and shape (form) of the specimen being investigated. The specimen is a thin 10-30μm thick foil with 10mm width and about 100mm length. It needs to be supported and held in place during the measurement, for which custom specimen holder is being designed. Taking into account these requirements, the solenoid is specified to be 500mm in length and 40mm in internal diameter. This size ensures homogenous magnetic field in the axis of the solenoid.

Because of the importance of the solenoid, computation model is developed to facilitate the design. The results can be seen in *Fig. 5*. The model gives the opportunity to quickly evaluate a huge number of solenoid parameter sets, and compare them in order to choose the optimal combination. It also helps in selecting the main pass element of the solenoid driver electronics that needs to control the solenoid current (see *Figure 6*). This pass element is a high power MOSFET, which has maximum power dissipation of around 80 – 90 Watts. This amount of power makes it necessary to mount the MOSFETs on heatsinks.

Fig. 5. Main data of solenoid, results from solenoid model

solenoid maximum voltage	30	V
solenoid length	500	mm
wire diameter	1,6	mm
layers of winding	6	-
solenoid core outer diameter	50	mm
Copper specific resistivity	0,017	Ohm*mm2/m
No. of turns per layer	306	
total length of wire	320,54	m
total mass of wire	5,8	kg
solenoid resistance	3,085	Ohm
maximum current	9,724	A
maximum H-field strength	35 707	A/m
H field resolution	0,5448	A/m/LSB
maximum power dissipation	292	W

Fig. 6. Power dissipation of the pass element and the solenoid in the function of solenoid current
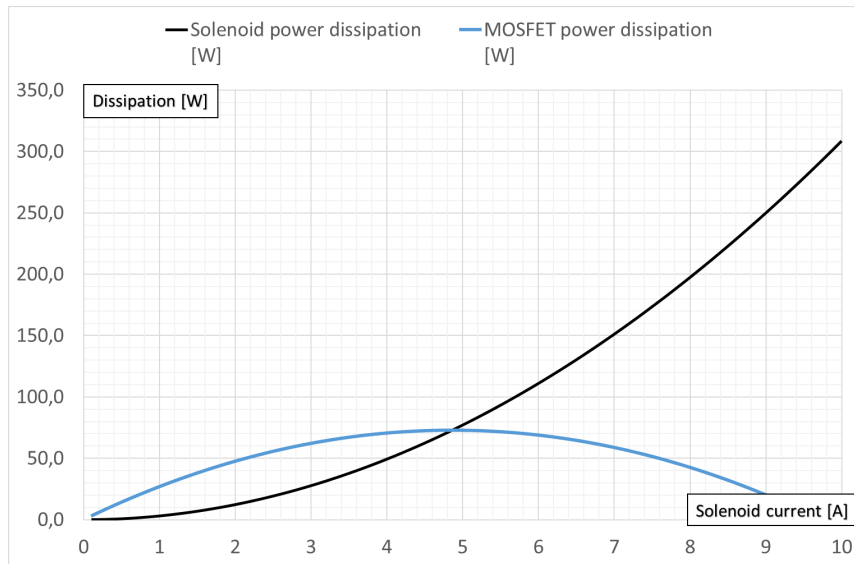
[1] Men, H., et.al. (2009): *Fe-Rich Soft Magnetic FeSiBPCu Hetero-Amorphous Alloys with High Saturation Magnetization, Materials Transactions,* Vol. 50. No. 6. Pp. 1330–1333.

Other key component is the magnetometer, which measures the B-field of the specimen. As explained in Chapter 2.2, fluxgate magnetometer sensors are selected for the application. The expected magnitude of the B-field is in the range of micro-Teslas, therefore the sensor measurement range is specified in ±10μT.

The control and acquisition electronics is responsible for driving the solenoid, collecting the data from the sensors and performing the necessary calibration and compensation to ensure high precision. The H-field range is specified in 25 kA/m with 0.1 A/m resolution. These values are also suggested by the literature. [1] The solenoid is excited with constant DC current that is precisely set by the electronics to satisfy the H-field specification.

Electrical design and challenges

The system control and acquisition electronics is designed with the specification in mind. The block diagram is shown in *Figure 7*.

Fig. 7. Control and DAQ electronics block diagram
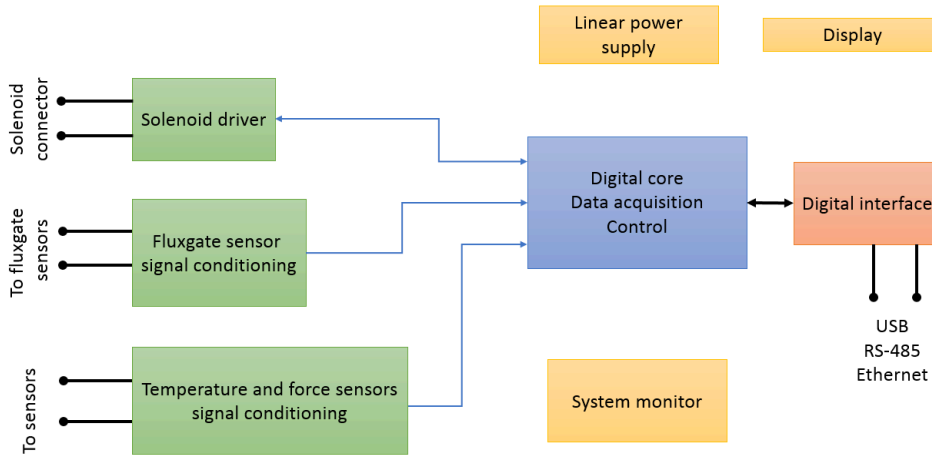
The most critical parts of the electronics in terms of effect on measurement accuracy are the solenoid driver and the signal conditioner of the fluxgate sensor. The solenoid driver must ensure accurate production of DC excitation current, in the range of 0 to 10 Amperes with 16 bit resolution. This, alone, would not satisfy the H-field range and resolution specification, therefore two selectable range is realized. For generating low magnitude H-field, the lower range can be selected which allows setting of a maximum of 2 Amperes of excitation current with 16 bit full range resolution. In the high range settings, the electronics is capable of produce the total of 10 Amperes of excitation current, also with 16 bit resolution. This switchable range selection is realized with solid-state electronics instead of electromechanical relays, therefore very low loss and leakage is ensured in the switching components. This fully solid state design also eliminates the minimum switchable current requirement of relays, that would make it impossible to drive mA of current through a high current capacity relay contact.

The mechanical design ensures the geometrical stability of the system. It is important to maintain high rigidity in order to allow accurate positioning of the specimen in the H-field, inside the solenoid. The materials used to construct the machine base and skeleton need to be antistatic, rigid, non-magnetic and non-conductive to prevent ground loop currents and other negative effects that could act as source of noise. Suitable materials are Bakelite or Epoxy resin based composites. If using of metal parts is inevitable, like for screws or sensor wiring, coper is the most suitable material due to its diamagnetic property.

Fig. 8. Control and DAQ electronics, mechanical design
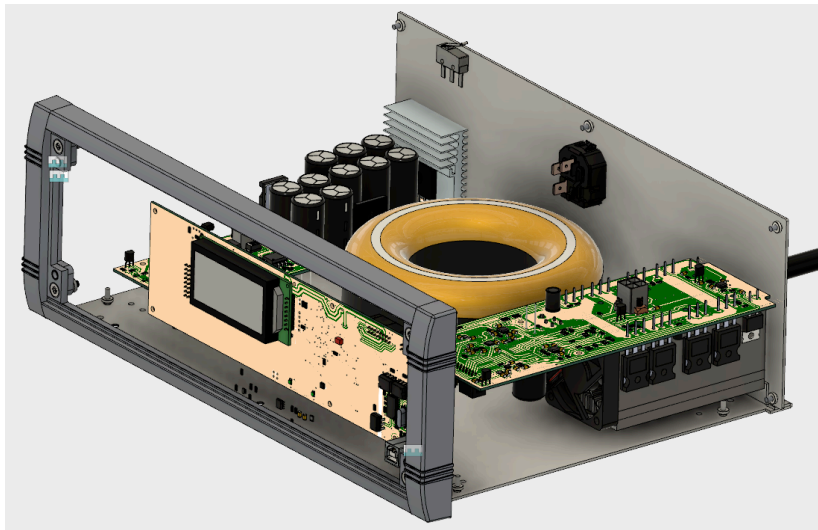
The main electronics is designed in an instrument enclosure by using 3D design tool as shown in *Figure 8*.

Summary

Conclusion

In this paper, some of the main challenges have been shown that arose in the design of magnetic properties measuring system. The system will be capable to determine the B-H curve and associated magnetic properties of small volume specimen, making possible to accurately determine the effect of different treatment of amorphous materials. The main challenge is to maintain the overall system accuracy at the specified level by ensuring accurate geometry, structure, and electrical design. The system is being designed using modern design tools, therefore the well documented design and construction is ensured.

MÁRTON NAGY *–KRISZTIÁN BÁN **–ÁGNES CZIRÁKI ***–ATTILA SZABÓ ****

The effect of laser cutting on the structure of amorphous glassy tapes

Abstract: Although thin metal strips or amorphous ribbons offer a higher magnetic performance compared to the presently used thicker crystalline electrical steels in electric motors, they have been considered unsuitable to build the rotor and/or the stator of classical electric motors because of fabricating limitations. Nowadays the development of high efficiency electrical motors has an outstanding significance, so an attempt is made to apply the soft magnetic glassy tapes to build stator and rotor elements for this application. However Fe based amorphous ribbons are promising base materials, but in order to use them, several additional requirements have to be satisfied, like cutting the soft magnetic elements into the appropriate shapes, avoiding the degradation (local crystallization) of the individual glassy elements. In this paper the heat affected zone of soft magnetic materials like FINEMET and METGLAS were examined after laser cutting. The investigations were focused on structural changes (XRD and DSC) and microhardness distribution of the heat affected zone which have a strong relation to mechanical properties for example embrittlement. These materials will be used in electric motors to increase its efficiency therefore it is important to us for later machinability and handling of laser cutted parts.

Keywords: Soft magnetic materials, heat affected zone, laser cutting, glassy alloys, amorphous alloys, FINEMET, METGLAS.

Összefoglalás: A fosszilis tüzelőanyagokat kiváltó gazdaságosabban előállítható és környezet kevéssé terhelő alternatív energiaforrások, mint például a villamos energia közúti közlekedésben való elterjedése elsősorban az energiatárolási nehézségek miatt még nem problémamentes. Szélesebb körű elerjedésének feltétele az egy töltéssel megtehető távolság növelése, és a jelenleg használt gépjárművek hatótávolságával összemérhető hatótávolság elérése. Ennek lehetséges módja az energiatárolás hatékonyságának növelése mellett

* *Budapest University of Technology and Economics, Department of Automotive Technologies*
E-mail: nagy.marton007@gmail.com

** *Budapest University of Technology and Economics, Department of Automotive Technologies*
E-mail: krisztian.ban@gjt.bme.hu

*** *Lorand Eötvös University, Department of Materials Physics*
E-mail: a.cziraki@freemail.hu

**** *University of Dunaujvaros, Institute of Engineering, Department of Mechanical Engineering*
E-mail: szaboattila@uniduna.hu

a járművek energiagazdálkodásának javítása. A járművek hatásfokjavításának egy lehetősége a járművek meghajtására szolgáló elektromotorok hatásfokának növelése. A korszerű anyagok és technológiák alkalmazásával a működés során keletkező veszteségek csökkenthetők: erre lehetőség az elektromotorok funkcionális (mágneses és elektromos vezető) anyagainak fejlesztése. Hatásfoknövelésre kínál lehetőséget a legmodernebb lágymágneses anyagok egy családja, a lágymágneses amorf ötvözetek Bár a vékony fémüveg szalagok mágneses jellemzői előnyösebbek a jelenleg ipari gyakorlatban használatos Fe alapú kristályos lemezek azonos tulajdonságaihoz képest, de azok megmunkálási nehézségei miatt hagyományos elektromotor forgórész/állórész építésére jelenleg alkalmatlannak bizonyulnak. Kutatásunkban a FINEMET és METGLAS típusú lágymágneses anyagokban a lézersugaras vágás hatására keletkező hőhatásövezetet, illetve annak kiterjedését vizsgáljuk. A vizsgálatokat elsősorban szerkezeti változásokra (XRD DSC) és mikrokeménység eloszlásra terjesztjük ki. Célunk a hőhatásövezet minimalizálása és a kristályosodási zóna szélességének csökkentése, annak megszűntetése.

Kulcsszavak: Alternatív energiaforrások, lézersugaras vágás, FINEMET, METGLAS, hőhatásövezet, amorf ötvözetek.

Introduction

Laser cutting of crystalline alloy plates are widely applied in automotive industry as an intermediated technological step in the production of body elements.

This process includes the local, well focussed melting and oxidation of Fe-based sheet elements, resulting measurable, well-matched surfaces.

It should be noted that laser cutting always includes a local thermal zone which presence is limited to the boundaries of plates. That is why it does not affect the strength of large body parts because it does not have an extensive effect on the crystal structure thanks to the dimensions and the equilibrium state of the crystalline plates. In contrast to cutting conventional sheet materials the laser cutting of metal glasses has many difficulties, although the laser application would be a great advantage in the elaboration of complicated workpieces. The main reason for this is the metastable nature of metallic glasses and the fact that laser cutting results in a considerable local heat effect leading to the local crystallization of metallic glasses which significantly undermines the chances of further processing.

Therefore, it has a great importance to study the area of thermal impact of laser cutting. This can be done mainly by local examination of the properties involved. The reason of this investigation that nowadays the world has been moving towards electro-mobility. Most of the research and development projects are focused on the efficiency enhancement of electro-motors. In cars mostly asynchronous motors are

used. One possible way is to increase the efficiency of electric motors to increase the operating frequency but this assumes that the loss of soft magnetic materials must be reduced. Therefore it should to replace the conventional FeSi soft magnetic materials to another type of soft magnetic material. Sheet elements made of Fe-based glassy or nanocrystalline alloys would be operated in asynchronous electric motor, as a part of the rotor and stator also, due to their low magnetic loss and high permeability. It is need to find the right manufacturing technology because its mechanical properties react very sensitively to heat caused by laser cutting, the structural relaxation and crystallization process indicates high fluctuation in hardness and causes embrittlement. In this paper we summarize the results of the hardness, DSC (Differential Scanning Calorimetry) and X-ray structure investigations in the heat affected zone of laser beam cutting.

Experimental

In this study $Fe_{73.5}Si_{13.5}B_9Nb_3Cu_1$, also known as FINEMET with an average thickness of 20 μm, and FeSiB or namely METGLAS with 25 μm were investigated. FINEMET and METGLAS ribbons were cut by a CO_2 type laser, OPL 2000 equipment, manufactured by Oerlicon. During the cutting process, argon protective gas was used to make the cutouts. The laser beam power was 60 Win a continuous mode, and it used 1200 mm/min laser beam feed rate.

The ribbons were tightly fixed with a strong adhesive tape, then 20-25 mm long and 10 mm wide parallel strips were cut out.

The first examination was the microhardness distribution measurement from the cut edge. Both material was measured by CSM Micro Combi Tester for Integrated Microhardness Meter and Microscope Analyzer. With a Vickers tip

80 pound load (784,8 mN with a 15 sec holding time) was applied during the measurements. The load was determined in a preliminary examination that the penetration depth does not reach the tenth of the ribbon thickness in the entire measurement process (as it is stated in the standard). It was carried out on the as quenched ribbon where the hardness was the lowest (therefore the penetration depth was the highest) in contrast to the expected results in HAZ. The preliminary examination had another role that our measurements could meet the conditions stated in the standard: minimal distance of the imprint center from the edge does not lower than 30 μm and between the imprint centers 40 μm. The environment of the cut edge had to be prepared for the measurements. Close to the cut edge on the surface of the FINEMET and METGLAS ribbons burr (in average diameter of cross section 40 μm) was formed after laser cutting. Near the generated line of the heat field when the diamond pyramid was approaching and penetrating in to the ribbon it stuck and slid on the burred surface under loading. In this case the measurement could

result an incorrect microhardness data. Thus, it was necessary to use P1000, then P2500 abrasive paper to remove the burr.

The second examination was the X-ray diffraction. X-ray diffraction measurements were carried out in the as quenched samples, strip samples removed from the closer environment of the laser cut edge and samples heat treated in isothermal conditions. Isothermal heat treatments (in 290°C, 340°C, 390°C, 450°C, 500°C and 600°C at 1 hour) were performed in order to compare the phase structure and properties of HAZ and conventionally (nano)crystallised samples. DSC examinations were performed to determine the exact conversion temperatures of the two types of amorphous alloys.

Results and discussion

The method of laser cutting is illustrated in *Fig 1.*:

Fig. 1. Laser cutting while moving the workpiece.
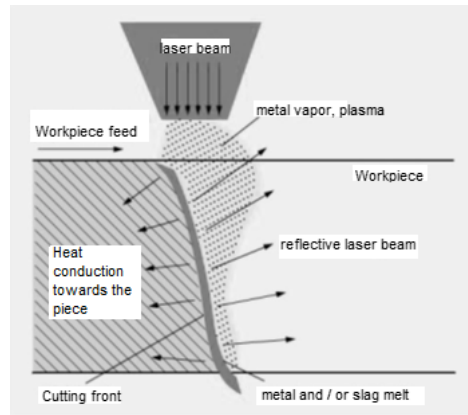
It is important to see that the cutting front is not vertical. It can not be possible because the melting of the material in the whole thickness of the plate requires time for the energy absorption from the laser beam. If the movement of laser beam to the workpiece stops, the cutting front would become vertical soon and the laser beam would pass through the plate without any absorption. At most, the small intensity of the beams edge would heat the edge of the cutting gap, but it would hardly melt it.

The focused laser beam is immersed on an inclined surface. The cut edge surface is rough. Its shape is primarily influenced by the intensity distribution within the focus.

Beyond the characteristics of the laser beam, there are additional factors like the physical, primarily thermal properties of the cut material, the viscosity of the melt and the gas flow conditions. The laser beam properties and the other factors (including the thickness of the cut material) determine how rough the cut surface will be.

Based on literature research, 5 stages of crystallization appear from the cut edge in the heat affected zone of amorphous soft magnetic materials.

Fig.2. The effect of laser cutting is expected to evolve different structure zones when cutting amorphous ribbons.
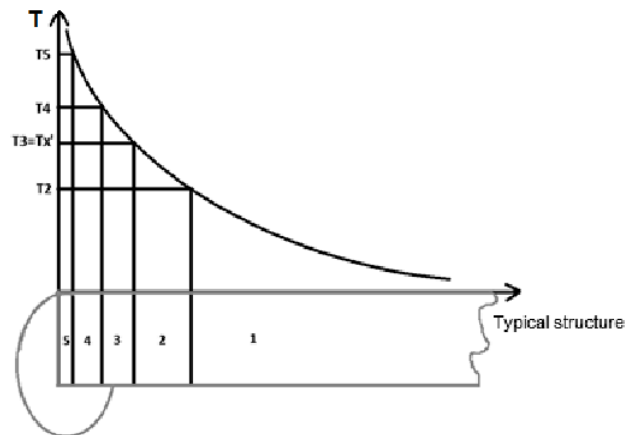
On *Fig. 2*, on the workpiece the burr is marked on the left. By this the individual phases of structural changes are numbered. In the zone 1 only structural relaxation of glassy state can be observed. According to the steps of the crystallization process, in zone 2 Cu-rich clusters are appeared. These two transition steps occure below about 450°C in the case of Finemet. In zone 3, the first crystalline phases are created (α-Fe (Si) + amorphous FeNbB) in the temperature range about 450–570°C at Finemet. Then, in the 4th and 5th zones (typically about 650–700°C and 700–750°C in the case of Finemet) the formation of borid crystalline phases is occurred.

It is expected that crystalline phases will emerge in the burr, but the mechanism of development is completely different, because here we could speak about melt crystallization.

[1] Herzer, G. (1997): *Handbook of Magnetic Materials.* (ed.) Buschow K. H. J. v.10. chapt. 3. Amsterdam: Elsevier Science. p. 415.

[2] Z. Weltsch, K.–Klam, A.–Lovas. (2017): The comparison hardness and coercivity evolution in various Fe-B based glasses (including FINEMET precursor) during relaxation and crystallization. *Acta Physica Polonica A* 131:(4) Pp. 669–671.

[3] Nagy, M. (2017): *Investigation of the introduction of nanocrystalline soft magnetic materials into the production of electromotors. Bachelor degree thesis.*Budapest.

For excellent magnetic properties it is need to achieve certain crystallization conditions. If the crystallization process is not stopped at step 3, the average grain size of the resulting α-Fe (Si) solid solution is larger than the desired 10 to 15 nm (being formed via primary crystallization) [1]. Consequently, the crystalline Fe borides increase the coercive force, and their appearance increase the magnetic loss (lower permeability and lower saturation induction) [2]. So, if this process occurs in the laser cut zone, it expands the magnetic hysteresis loop of the glassy alloy in this environment.

On *Fig. 3*, it is clear to see some cracks and brakes in which the local rigidity is reflected [3]. Due to the laser cutting the higher temperature hardened the material (which had a high initial hardness), therefore it becomes easily breakable.

Fig. 3. Photo of refined laser-cut zone of FINEMET ribbon with breaks (1) and cracks (2).
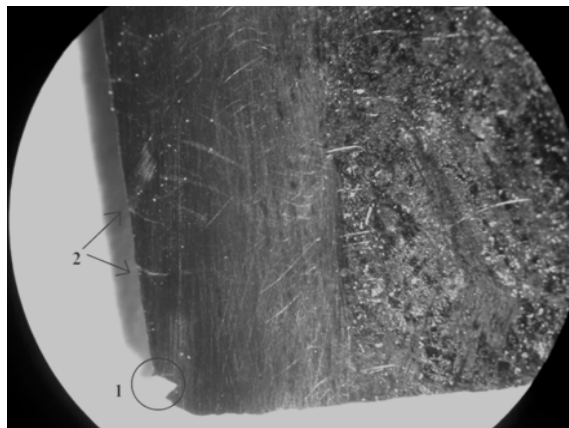
Vickers microhardness are measured of FINEMET and METGLAS ribbons before and after the laser beam cutting.

[3] Nagy, M. (2017): *Investigation of the introduction of na-nocrystalline soft magnetic materials into the production of electromotors. Bachelor degree thesis.* Budapest.

Fig. 4. The microhardness values of FINEMET ribbon after laser cutting versus the distance from the cut edge.
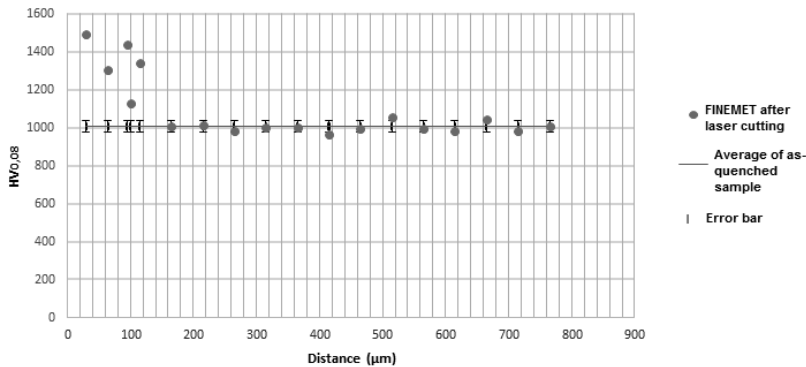
On *Fig. 4* [3], the average of basic hardness of FINEMET (1000 HV0,08) ribbon was marked with line "Average of as quenched sample". Deviation from this was marked by error bar. 30 μm from the edge, the first imprint was measured, which was 1492 HV0,08 hardness. By increasing distance, the hardness values had a high fluctuation. When it was around 150–200 μm from the edge, it reached the initial hardness. Accordingly, the heat affected zone of FINEMET ranges from 0,15 to 0,2 mm [3]. METGLAS ribbon was also measured by the same conditions that is shown on *Fig. 5.* [3].

Fig. 5. The microhardness values of METGLAS ribbon after laser cutting versus the distance from the cut edge.
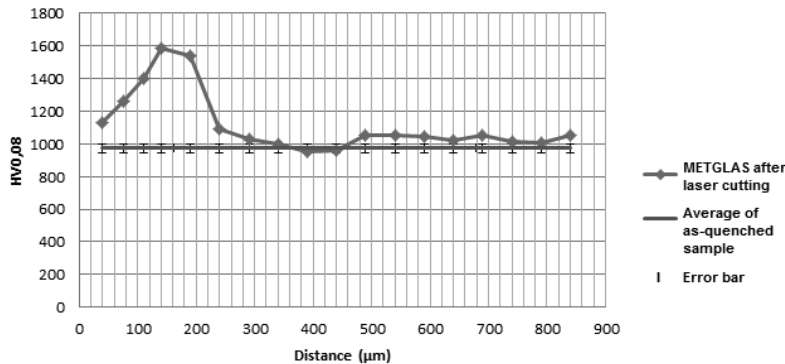
[3] Nagy, M. (2017): *Investigation of the introduction of nanocrystalline soft magnetic materials into the production of electromotors. Bachelor degree thesis.* Budapest.

[4] J. *Less-Common Met.* 1988, 142., Pp. 91–104.

[5] *Phys. Rev. B. (*1986): *Condens. matter* 34., Pp. 4738–4743.

After an initial growth at 150 μm from the edge of the material (when measuring the 2nd imprint) the highest hardness was measured with 1597 HV0.08. Continuing it started to gradually decrease and its value around 300 μm reached the basic hardness. Thus, its heat thermal affected zone ranges from the edge of the plate to 0,3 mm [3].

Based on the hardness values we can assume the appearance of Cu-rich clusters and the phenomenon of crystallization, but the boundary of the zone can not be separated. Therefore we carried out isothermal heat treatments on which we planned to perform paralell measurements of microhardness and XRD examination. On the beginning of the heat affected zone, the reason for the measured lower hardness is unclear.

On *Fig. 6* [3], there is a METGLAS sample with some imprints (20x optical zoom). The ribbon is scratched because abrasive paper was used to remove the burr. On the sample it is visible that there is a row with polygon imprints from the cut edge.

The size of their shape is getting bigger from the cut edge because near to the edge of the sample it was harder to make imprints thanks to the hardening effect.

Fig. 6. Imprints on METGLAS sample with 20x optical zoom.

The XRD measurements of commercially available METGLAS and FINEMET samples showed amorphous structure and homogenous in the whole volume (*Fig 7. a*). The XRD image of strips taken from the FINEMET sample cutted with laser is shown in *Fig. 7. b*. In addition to the broad amorphous maximum, sharp crystalline peaks emerged which arised from the HAZ of laser cut surface and from the burr also. On the basis of the lines, some of them correspond to the Fe3Si phase but the FeB [4, 5] phase and even the Fe-O phases are present in this crystalline environments.

Fig. 7. XRD graphs of FINEMET sample a) in as quenched state b) strip from HAZ caused by laser cutting.

a)   b)
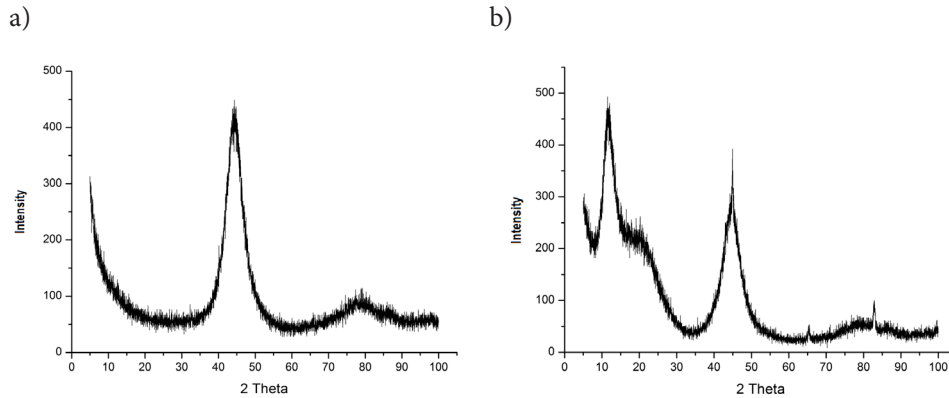
After isothermal heat treatments at 290°C, 340°C and 390°C samples were amorphous there were no detectable changes with XRD measurement. In these temperatures only structural relaxation was possible. The crystallization starts at 450°C and develops further at 500°C, the lines were sharpened and their intensity increased it means that their amorphous fraction decreased (see *Fig. 8*.). Compared to the literature data we found that the vast amount of crystallites formed correspond to the Fe3Si phase. Due to the 600°C heat treatment the lines familiar to the sample heat treated at 500°C. The lines are barely changed.

Fig. 8. XRD graphs of FINEMET sample heat treated at isothermal conditions at 390°C and 450°C (after 450°C sharp peaks appeared).
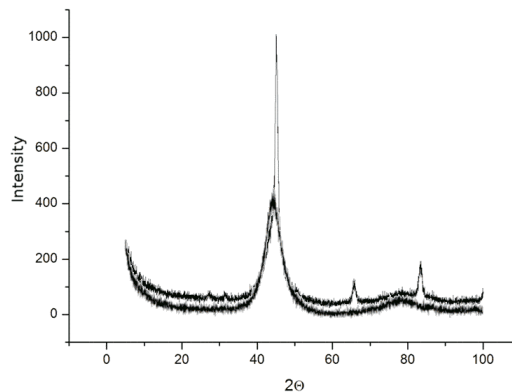
From the XRD results, unfortunately, it is impossible to separate that the crystalline environments formed in the burr which newly crystallised from melt or formed in the HAZ by crystallisation of the amorphous state.

As described above the transition stages have specified temperature ranges in the case of defined type of alloy. For the exact determination of the transformation temperatures for the given samples DSC examinations were performed.

Fig. 9. DSC graphs of a) FINEMET and b) METGLAS samples.
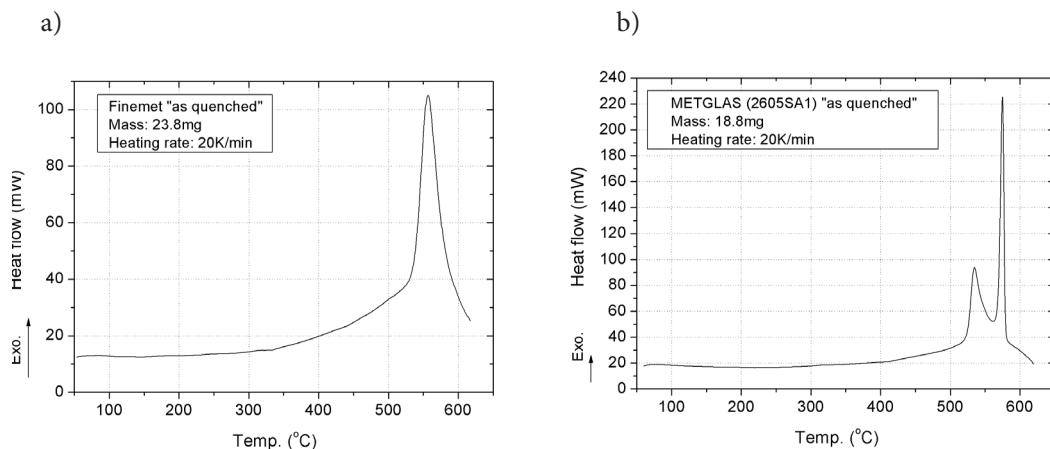
At the FINEMET sample from 350°C an exoterm heat effect could be observed which refer to a short range reordering: structural relaxation and formation of Cu-rich clusters but the two process can not be separable (see *Fig. 9. a)*.

The crystallisation process initiated around 530°C with heating rate 20 K/min. This showed a significant delay compared to the XRD results (at samples treated at 450°C we fuond crystalline phases) but it should be noted that XRD measurements carried out in samples heat treated in isothermal condition.

At METGLAS sample the exoterm heat effect initiated around 412°C (see *Fig. 9. b*). Two crystallisation set up could be observed at around 521°C and 562°C. The second crystallisation stage at FINEMET was not observed below 600°C thanks to Nb content which give a delay in the second crystallisation process.

Summary

The extension of heat affected zones is studied in laser cut FINEMET and METGLAS ribbons. The width of this zone is typically 150-250 µm depends on the base material. At the very vicinity of laser cutting, melted formation was observed in this zone. Ribbons rigidity was observed arising either from local crystallization or structural relaxation. This type of rigidity makes it difficult to use in electric equipments. During laser beam cutting other parameters should be tried in order to ascertain that this cutting technology is the relevant or not for these soft magnetic materials. There is a need to examine the structure of FINEMET and METGLAS ribbons after water jet cutting too. For the separation of phases in HAZ by microhardness results the microhardness measurements of the isothermal heat treated samples are necessary.

Acknowledgement

ANTAL LOVAS *–ATTILA SZABÓ **

Difficulties in 3D metal printing: The inner stress evolution due to non-equilibrium phase transformation

Abstract: Recently an attempt is made to apply the 3D printing to build customized devices; however, during the manufacturing a stress development has been found which limitates the lifetime of the products. In this paper some basic metallurgical considerations are applied in order to enhance the deeper understanding the origin of such stress evaluation phenomena. The significance of local, rapid solidification is emphasized, which is coupled with reduction of solute rejection, resulting the formation of non-equilibrium supersaturated solid solution within a solid volume elements. The supersaturated solid solutions are inherently metastable around room temperature, which are capable to result local deformations even in the completed 3D printed parts.

Keywords: 3D printing, non-equilibrium solidification, local stress evolution, supersaturated solid solution.

* *Budapesti Műszaki és Gazdaságtudományi Egyetem*
Email: antal.lovas@gjt.bme.hu

** *Dunaújvárosi Egyetem, Műszaki Intézet*
E-mail: szaboattila@uniduna.hu

Összefoglalás: A 3D-s nyomtatás jelentősége a napjainkban egyre növekszik, melynek okai a növekvő és szigorodó ipari elvárások, valamint a prototípusgyártásra szánt szűkebb határidőkben keresendők. Bár a 3D-s nyomtatás során a kapott késztermék alakhűsége és funkciónális jellemzői kiemelkedők, de a gyártás során keletkező belső feszültségek idővel az alkatrész deformálódásához, repedéséhez vezethetnek, csökkentve ezzel az alkatrész élettartamát. Munkánk során ezen belső feszültségek kialakulásának a metallurgiai hátterét vizsgáljuk. E feszültségek kialakulásában kiemelkedő jelentősége van nyomtatott olvadékcsepp gyors megszilárdulásának, ugyanis a gyors hőelvonás során a diffúzió sebességének lecsökkenése következtében csökken az oldott atomok kiválása, ami a nem egyensúlyi túltelített szilárd oldat kialakulását eredményezi egy szilárd térfogatú elemeken belül. A túltelített szilárd oldatok természetüknél fogva metastabilak a szobahőmérséklet

[1] Hendra, H. (2011): *Metals for Biomedical Applications.* Biomedical Engineering. From Theory to Applications Intech.

[2] Takács, J. (2017): *Additive Manufacturing of Customized Human Implants and Medical Device.* „GÉP" LXVIII. Pp. 16–22.

[3] Boettinger, W. J. (1993): *Fundamantals of solidification at high rates in rapidly solidified alloys.* Marcel Dekker Inc.

[4] Thijs, L. (2010): *A study of the microstructural evolution during selective laser melting. Acta Materialia.* 58/9. Pp. 3303–3312.

körüli hőmérséklettartományban, amelyek akár a befejezett 3D nyomtatott részeken is képesek helyi deformációkat okozni.

Kulcsszavak: 3D-s nyomtatás, nem egyensúlyi, szolidáció, helyi stressz-evolúció, túltelített szilárd oldat.

Introduction

In the development of 3D printing (motivated by the demands from the rapid prototyping, human implants, medical devices, etc.) the selective laser melting is often use to build up nearly net shape geometries. [1] The raw materials in these technologies (especially in the case of metallic implants) generally two or-multi-component alloy powders with different physical properties (i.e. melting point, specific heat, emission coefficient etc). [2] This technology involves many laser scanning through different, neighbouring scan vectors. [3]

During this successive laser scans, several independent (at least partially coupled or overlapped) physical effects are responsible for the quality of implants. These can either enhance or restrict the applicability of the products. Some of the production factors are associated with the highliy localised thermal effects, arising from the heat inputs, resulting also very short interaction times between the component metal particles. As a consequence, the development of special, non-equilibrium phase relations are expected.

The perfect physical continuity of solidified structure can also be influenced by the interfacial phenomena, i.e. the wetting characteristics between the neighboring liquid-solid phases. This is sensitively depends even on the traces of gas adsorption, due to the high specific surface associated with the individual, highly dispersed components (alloy powders). [4]

Cooling rate and local thermal temperature gradients between the interacting metallic phases or the individual grains has also a dominant role in the evaluation of phase relations (i.e. the degree of possible deviation from the thermodynamical equilibrium circumstances)

A secondary (mainly diffusion controlled) phenomena can be also evaluated in solid state between the interacting non-equilibrium volume elements. Such phenomena are thermally activated and influenced by the repeated heat effects (heat shocks) caused by the subsequent temperature change (subsequent laser scan).

In the present paper mainly the possible role of non-equilibrium nature of the solidification, will be discussed.

[3] Boettinger, W. J. (1993): *Fundamantals of solidification at high rates in rapidly so-lidified alloys.* Marcel Dekker Inc.

The formation of non-equilibrium phases during Selective Laser Melting (SLM)

The raw materials of SLM technology are dominantly multicomponent metallic powders in which the number and concentration of equilibrium phases is governed by the Gibbs phase rule.

While the equilibrium phase relations are developed at very low cooling rates, these „equilibrium solidification circumstances" usually not fulfilled during the SLM processes. Here, usually pulse-like local heating and subsequently, also rapid heat extraction occur (rapid solidification and, consequently non-equilibrium solid phases are frozen). The non-equilibrium conditions during the rapid solidification are characterized by the velocity dependent distribution coefficient ($K(v)$) between the solidifying liquid and the contacting solid phase according to

$$K(v) \cdot \frac{K_0 \cdots \beta_0 \cdot v}{1 \cdots \beta_0 \cdot v} \qquad (1)$$

where β_0 is a system-dependent constant. It means, that $K(v)$ depends on the velocity (v) of the solidification front. By increasing the solidification rate to infinite ($v \rightarrow \infty$), the $K(v) \rightarrow 1$. While decreasing the solidification rate to zero ($v \rightarrow 0$), the $K(v) \rightarrow K_0$ (equilibrium distribution coefficient, which is illustrated in *Fig. 1*).

According to *Fig.1.*, during equilibrium solidification, the concentration of liquid and solid phase shift along the solidus and liquidus line respectively, as the temperature is lowered (equilibrium phase diagram).

In contrast, the (equilibrium) distribution is never fulfilled, when the liquid phase is supercooled due to the rapid heat extraction. This situation is shown in *Fig.2*, where the maximum degree of supercooling is illustrated by the T_0 curve. Along this curve the temperature dependence of concentration for the supercooled liquid and the solid phase is identical, i.e. the liquid can solidify without solute rejection at the crossing point of T_0 and C_L. [3]

[3] Boettinger, W. J. (1993): *Fundamantals of solidification at high rates in rapidly solidified alloys.* Marcel Dekker Inc.

Fig. 1.Effect of the distribution coefficient upon solute rejection. [3]
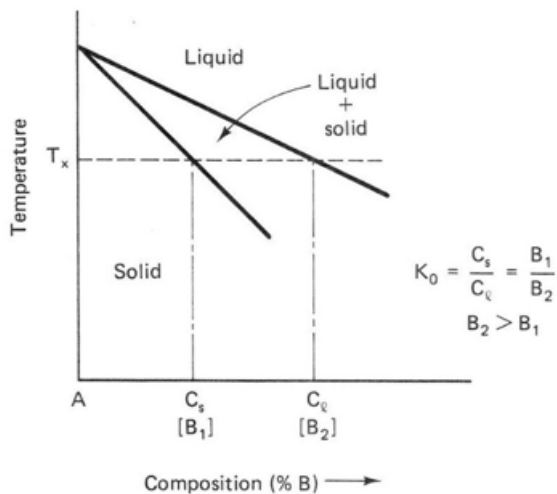
Fig. 2. Regions of thermodynamically allowed solid composition that may be formed from liquid of composition CL at various temperatures. [3]
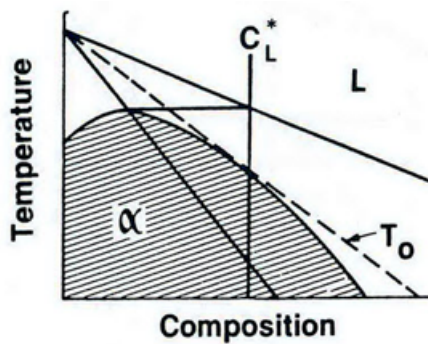
Fig. 3 Schematic representation of T0 curves for the liquid to crystal transformation in eutectic systems, forming supersaturated solid solutions at high melt undercolooling (high cooling rate). [3]

[3] Boettinger, W. J. (1993): *Fundamantals of solidification at high rates in rapidly so-lidified alloys.* Marcel Dekker Inc.

[4] Thijs, L. (2010): *A study of the micro-structural evolution during selective laser melting. Acta Ma-terialia.* 58/9. Pp. 3303–3312.
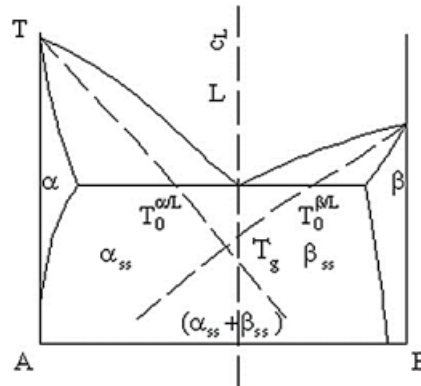
In *Fig. 3.* an eutectic system is shown with limited solubility. According to the appropriate T_0 curves belonging to a non-equilibrium (partionless) phase trans-formation, in the eutectic crossing point two supersaturated solid solution are in equilibrium. The concentration of supersaturated solid solutions (α_{ss} and β_{ss}) obvi-ously differ from the appropriate equilibrium of α and β. phases being formed at the temperature of eutectoidal. According to the outlined principles, the following tendencies can be expected during the high undercooling, fulfilled either by SLM technology. As the supersaturated solid solutions compositionally metastable, they tend to decompose at low temperatures (around room temperature).

The activation energy for the precipitate (new phase) formation is supplied by the transient warming up during the formation of neighboring layers.

The dimension of the precipitations (new phase formation) which are typically in the range of several micrometers, depend on the local (process dependent) tem-perature gradient and also influenced by the hatching spaces applied during the layer formation. [4]

[5] Turnbull, D. (1981): *Metastable structures in metallurgy. Metallurgical Transitions B.* 12B. 217.

Fig. 4. Examples for alloying elements, which enhance the austenite(fcc) and inhibits the ferrite (bcc) phase stabilization in Fe-host metal.
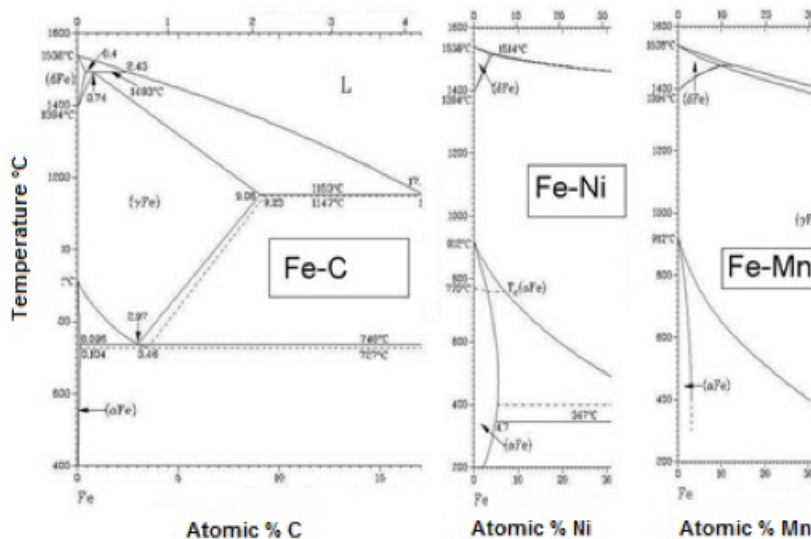
(ASM Alloy Phase Diagram Database)

The supercool ability highly depends also on the shape of appropriate phase diagrams which is complicate. Therefore, provide indirect information only. Some indirect tendencies can be subtract from the shape of appropriate binary phase diagrams, as it is shown in the *Fig. 4 and 5*.

The frozen supercooled phases can be metastable either compositionally or, structurally. Both metastability types may also occur simultaneously at room temperature. [5]

The alloy components are divided into two groups. Some alloy components tend to stabilize the fcc (γ) phase:, like the C, Ni or Mn while others initiate the extension of α region either in high or low temperature range (ferrite or austenite/forming elements). In the case of austenite-forming elements the stability range of γ phase is extended to room temperature, therefore, neither chemical nor structural driving force or new phase nucleation do exists. Low temperature transformations in the

case of ferrite forming components is more pronounced, because the entrapped austenite is metastable around room temperature range, consequently such compositions are more sensitive to the transient temperature increase or also to the stress induced transformations. Examples for such ferrite-forming elements are collected in the *Fig. 5.*

In these figures (*Fig. 4. and 5.*), the sections of binary phase diagrams can be compared in the case of austenite or ferrite stabilizing elements.

Trapping of high temperature stable phase nuclei may occur, when fcc and bcc stabilizer components are often simultaneously present in the alloy produced by. [6]

The possibility of such solid-solid transformation, (even without compositional change) can be the source of stress center formation, due to the different density of phase volume elements. Local discontinuous density change can be developed in such alloys, resulting even macroscopic deformation or the fatigue of products.

[6] Kruth, J. P. (2004): *Selective laser melting of iron-based powder.* Journal of Materials Processing Technology. 149. Pp. 616–622.

Fig. 5. Examples for alloying elements, which inhibit the austenite(fcc) and enhance the ferrite (bcc) phase stabilization in Fe-host metal.
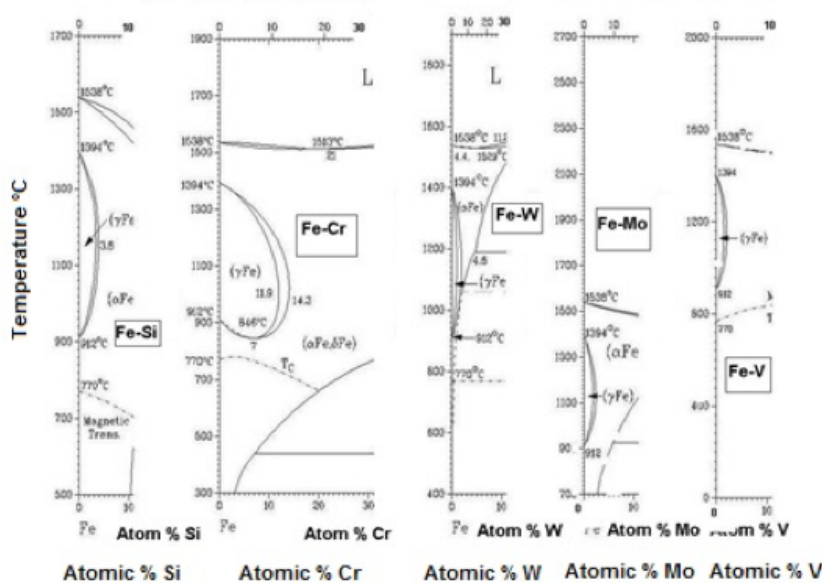
(ASM Alloy Phase Diagram Database)

Discussion

Opposite to the traditional melting and casting processes, where the usual cooling rate of the melts are in the magnitude of 102 K/sec, the local chemical and physical fluctuation can be developed in the magnitude of hatch spacing during the SLM process. As a consequence of the highly localized heat inputs, high temperature gradients are developed, resulting non-equilibrium segregation within the small volume of solidified alloy.

The resulting locas stresses may iniciate crack formation causing harmfull integrity problems and finally the stability decrease of the products.

Summary

The following conclusions can be drawn from our research:
– The formation of non-equilibrium segregation is inevitable during the SLM process, due to the local, short time pulse-like heating and cooling of the melt pool.
– Microscopic discontinuities, pore formation -which is the consequence of unsufficient wetting circumstances between- the powder components, decreasing also the integrity of implant elements.

Acknowledgements

Galéria

Duma Bálint fotói (Albánia 2018)